International Journal of Humanoid Robotics
Vol. 14, No. 4 (2017) 1750010 (21 pages)

DOI: 10.1142/S0219843617500104

Mechanism Design of a Humanoid Robotic Torso Based on Bionic Optimization

Peng Yao[*,†,§], Tao Li[†,¶], Minzhou Luo[‡,‖], Qingqing Zhang[*,†,**] and Zhiying Tan[†,††]

[*]*Department of Precision Machinery and Precision Instrumentation, University of Science and Technology of China, Hefei 230022, P. R. China*

[†]*Hefei Institutes of Physical Science, Institute of Advanced Manufacturing Technology, Chinese Academy of Sciences, Changzhou 213164, P. R. China*

[‡]*Hefei Institutes of Physical Science, Chinese Academy of Sciences, Hefei 210031, P. R. China*

[§]*ypstyle@mail.ustc.edu.cn*
[¶]*roboylee@163.com*
[‖]*lmz@iim.ac.cn*
[**]*qqzhang@mail.ustc.edu.cn*
[††]*zytan@iamt.ac.cn*

Received 6 September 2016
Accepted 30 January 2017
Published 11 April 2017

A new torso structure for a humanoid robot has been proposed. The structural characteristics and functions of human torso have been considered to gain inspirations for design purposes. The proposed torso structure consists of six revolute units divided into two basic categories connected in a serial chain mechanism. The proposed torso structure shows more advantages compared to traditional humanoid robots in terms of high degrees of freedom (DOFs), high stiffness, self-locking capabilities, as well as easy-to-control features. Bionic optimization design based on objective function method has been implemented on structural design for better motion performances. A 3D model has been elaborated and simulated in SolidWorks and ADAMS environments for structural design and kinematic simulation purposes, respectively. Simulation results show that the new bionic torso structure is able to well imitate movements of human torso.

Keywords: Humanoid robot; human spine; torso structure; mechanism design; bionic optimization.

[¶]Corresponding author.

1. Introduction

Humanoid robots are robots with their body shapes built to resemble the human body. Therefore, they can adapt to human living environment, make use of tools and get along with people with affinity for their appearance and size. Generally, single leg and single arm are designed with six degrees of freedom (DOFs) to achieve various movements in three-dimensional space. Nevertheless, spine structure has not been effectively incorporated into the design of humanoid robotic torso. More than 90% of proposed humanoid torsos are greatly simplified as waist joints with 1–3 DOFs, very few with four DOFs.

The torso of ASIMO[1] which is on behalf of the most advanced technology in humanoid robots only has a rotary joint (Roll) in transverse plane; KHR[2,3] and HUBO[4,5] series built at KAIST have a rotational DOF(Yaw) in waist. HRP[6–8] series developed at AIST set up two DOFs (Pitch-Yaw) in waist; iCub[9] of IIT has three DOFs (Roll-Pitch-Yaw) in torso; WABIAN-2[10] developed at Waseda University has four DOFs (Roll-Yaw-Pitch-Yaw) in waist and torso; Myon[11] of Humboldt University adopted a rotary joint (Roll) in waist. In addition, BHR-2[12] built in the Beijing Institute of Technology has been designed with a box-like shape torso of zero DOF; IRP-1[13] developed by Hefei Institutes of Physical Science has two DOFs (Pitch-Yaw) in torso.

Some researchers attempted to design torso structures for humanoid robots with inspirations of human torso. Or has done some research on WBD-2[14] with highly anthropomorphic torso structure by using six servos connected in series in Takanishi Laboratory. WBD-2 aimed to express emotions by using body languages. However, torso structure with six servos connected in series simply did not achieve various excellent properties of spine but better flexibility. Holland team in University of Essex developed CRONOS[15] with imitation of human skeletal structure, and ECCEROBOT[16] based on CRONOS was developed by Sussex University, Technical University of Munich and University of Zurich. This robot has an anthropomorphic design from appearance to internal structure. However, intrinsic movement patterns and control methods to achieve various motions still are urgent problems to solve. Musculoskeletal flexible-spine humanoid robots named as Kotaro,[17] Kojiro[18] and Kenshiro[19] built at JSK laboratory of Tokyo University with high redundancy have five ball joints connected in series in waist to simulate spine and adopt a large number of artificial muscles, which achieved bending and some delicate movements successfully. But it is very difficult to control robots to achieve stable walking and collaborative actions involved in the whole body, and its stiffness is low since there is no evidence shown that it can stand without external force. Some cable-driven torsos[20,21] have same disadvantages.

Torso design for humanoid robots mentioned above have already achieved certain results. The main disadvantages include the following aspects: firstly, oversimplified bionic spine mechanisms are failure to achieve various properties of human spine; secondly, torso structures with highly anthropomorphic spine and muscle groups are

difficult to achieve the goal of effective control. The purpose and contribution of this paper can be recognized as solving these urgent disadvantages. In this paper, the performances of human torso in mechanism and motion patterns have been investigated, and a new torso structure for a humanoid robot has been proposed based on general six revolute (6R) serial mechanism. Bionic optimization design based on physiological parameters of human torso has been carried out to demonstrate the practical feasible operation performances of the proposed torso structure. A 3D model has been elaborated in SolidWorks environment and simulation results are reported to present the characteristics of torso structure.

2. Analysis of Human Torso

The unique structure of human spine is the result of long-term evolution. Humanoid robots are inspired by structure and motion capabilities of human body for better adaptability in human social environments.[22] Therefore, it is necessary to investigate characteristics for humanoid robotic design.

The vertebral column begins at the support of the skull and ends with an insert into the hip joint. Thirty bones in series constitute the vertebral column: cervical (C1–C7), thoracic (T1–T12), lumbar (L1–L5), sacrum (S1–S5) and coccyx.[23] It protects the spinal cord and provides a firm support for torso, head and upper limbs.

As shown in Fig. 1, the spine of an adult features four sagittal curves, namely they are cervical, thoracic, lumbar and sacral curves. The curvature angles of cervical, thoracic, lumbar curves reach to $\alpha\,(21.9^\circ), \beta\,(30.9^\circ), \gamma\,(31.4^\circ)$, respectively.[24] Curvature is an important physiological functionality of spine, it is qualified for the role of keeping the mass center of torso close to the longitudinal axis so that human can maintain balance because of its relative positions between adjacent vertebrae. Torsos with curvatures provide more than 10 times of strength and resilience compared with straight vertebral column.

Various motions of human body can be summarized as complex combinations of three typical motions including flexion (or extension), lateral bending and rotation. Flexion and extension occur in the sagittal plane around the frontal axis. Lateral bending occurs in the frontal plane around the sagittal axis. Rotation occurs in the transverse plane around the vertical axis. Though motion degrees between adjacent vertebrae are different, the entire spine with 30 vertebras in series shows larger workspace. The amplitudes of these movements are shown in Fig. 2.

From the microscopic point of view, three motion patterns between adjacent vertebrae also can be reflected. As shown in Fig. 3, specific motions are achieved via alignment of the facet joints and the attaching spine muscle, which subsequently generate force to move corresponding vertebrae and accomplish predetermined motions.[25] Stability of torso also mainly depends on muscles and ligaments. For example, when shaking your head in disagreement, the rotation of the head controlled by the atlantoaxial joint between C1 and C2 can be realized.

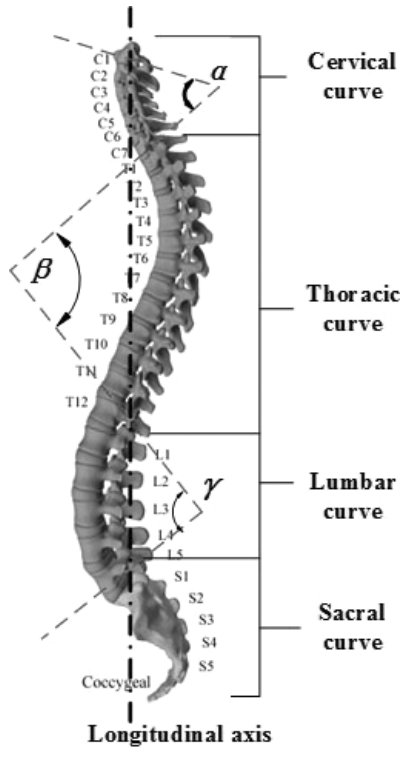

Fig. 1. Human spine structure.

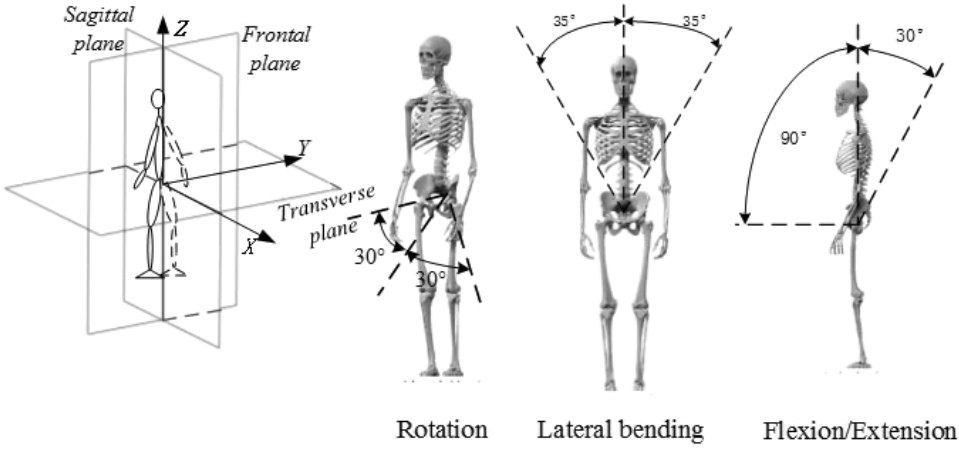

Fig. 2. Typical human body movements and the corresponding amplitudes. Spinal flexibility is considerable for these movements and larger workspace.

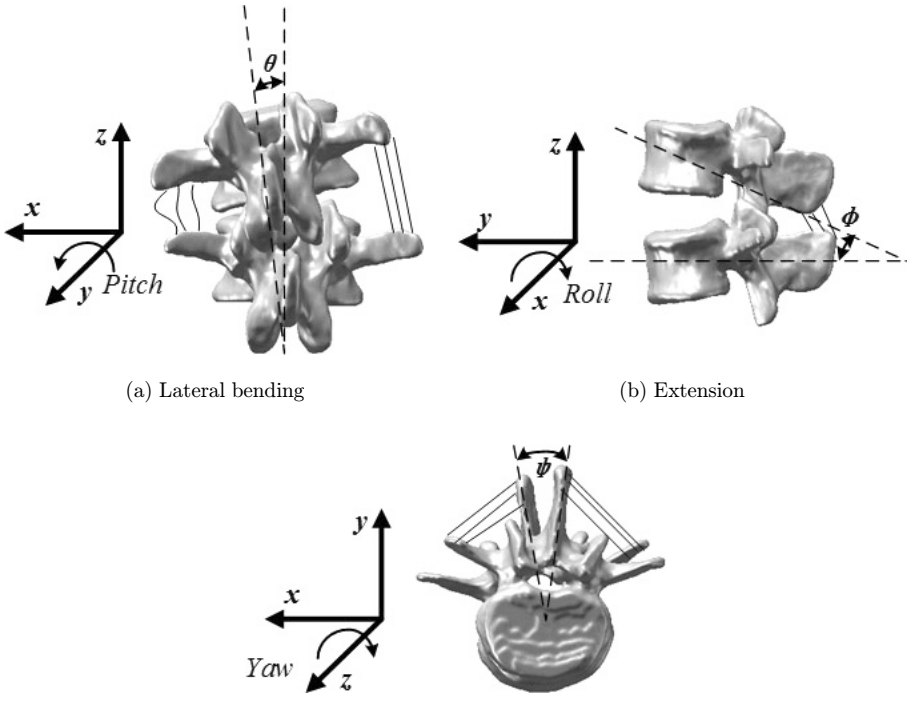

(a) Lateral bending

(b) Extension

(c) Rotation

Fig. 3. Typical motion patterns in microscopic form, the line of pull represents the erector spinae muscles determine actions and stability of spine.

It is summarized that three representative torso design requirements for humanoid robots from the analysis of structural and motion characteristics of human torso: firstly, high flexibility. Complex motions of spine in 3D space depend on multiple DOFs of the serial system; secondly, large workspace. Human body can achieve large workspace in collaboration with spine; thirdly, stability and stiffness. Human body withstands considerable force while moving, physiological curvature helps body reduce concentrated force and keep the body stable. In terms of mechanism design, it requires a certain rigidity to withstand forces acting on it. In addition, a relatively simple control method to achieve above requirements is worth considering.

3. A New Torso Structure for a Humanoid Robot

In Fig. 4, a new torso structure for a humanoid robot is illustrated in a 3D model that has been elaborated in SolidWorks environment. R1 connects to the pelvis platform, and R6 connects to the head of a humanoid robot.

The proposed torso structure consists of six units marked as R1–R6 from the bottom to the top, which are connected together in series. Six units can be divided

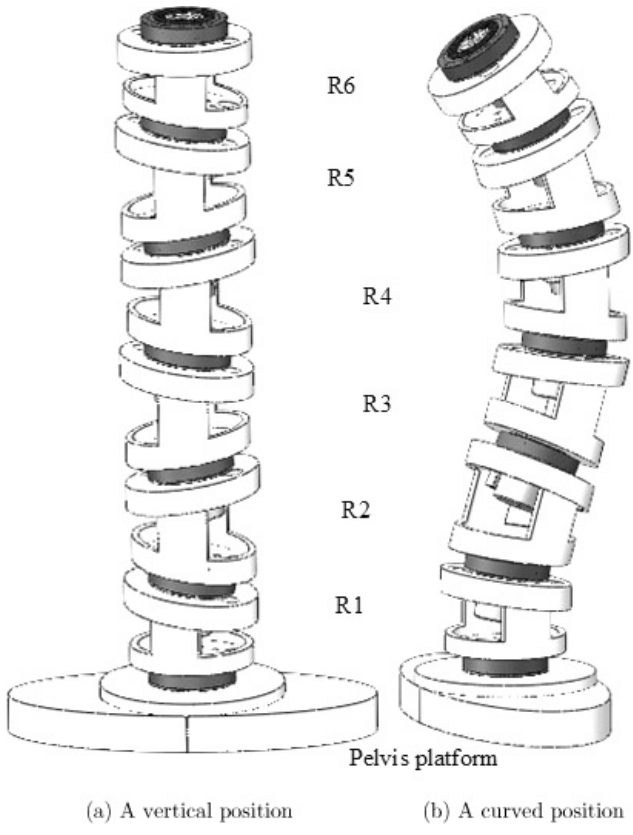

Fig. 4. A 3D model of a humanoid robotic torso.

into two basic models as shown in Fig. 5. Internal components are substantially same including harmonic reducer, motor, output flange sleeve, input flange cover, actuator and encoder. The difference is the angle between output flange sleeve and input flange cover, it decides the location of rotation axes and subsequently decides motion results. R1 and R6 are in the form of Module 1, the rest are in the form of Module 2.

Module 1 is designed for better connections with the head and the pelvis platform, which will make humanoid robots keep stability during movements; The design principle of Module 2 is seeking for achieving the desired operation performances of bending angles with fewer units, so angle between output flange sleeve and input flange cover is the double of Module 1's. Harmonic reducer is used to connect adjacent units, and this kind of method is good for the compact and rigidity of torso structure.

Structural characteristic is analyzed from the perspective of DOFs configuration. Figure 6(a) shows the general 6R serial mechanism with irregular configuration of DOFs. Industrial 6R serial robots usually have the spherical joint with three joint axes intersecting at one point in order to solve analytical solution of inverse

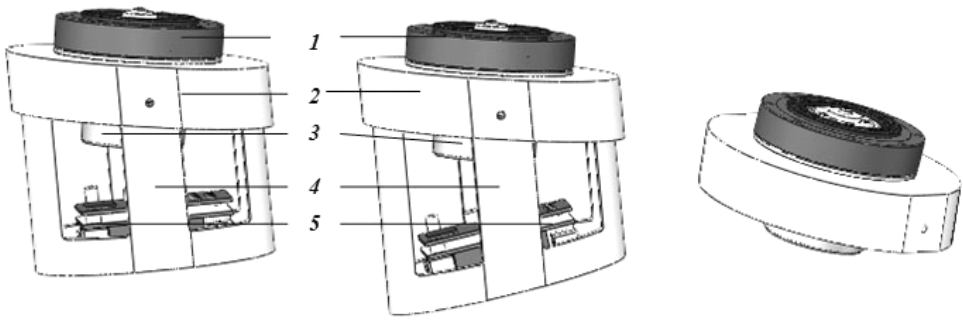

(a) Module 1 (b) Module 2 (c) A connecting portion

Fig. 5. Components of the proposed torso structure: 1: Harmonic reducer; 2: Input flange cover; 3: Motor and encoder; 4: Output flange sleeve; 5: Drive motor.

kinematics,[26] and most joint axes are in orthogonal relationship. For the proposed torso structure of humanoid robot, these joint axes are not orthogonal, and angles (α) between adjacent joint axes presenting with regular alternative distribution are not equal to $0, \pi/2$ or π as shown in Fig. 6(c). Particularly, no spherical joint exists in the proposed torso. In a vertical position, axes of six joints are in the same plane. Bionic performance is fully considered for adopting this design. For example, the proposed torso structure presents a continuous curvature during bending motion compared to traditional robots with only consideration of the appropriate posture of head, the movements are unnatural.

Typical unit of general 6R serial mechanism is composed of joint and link, and link rotates around the joint. For humanoid robots, space for torso part is limited. The

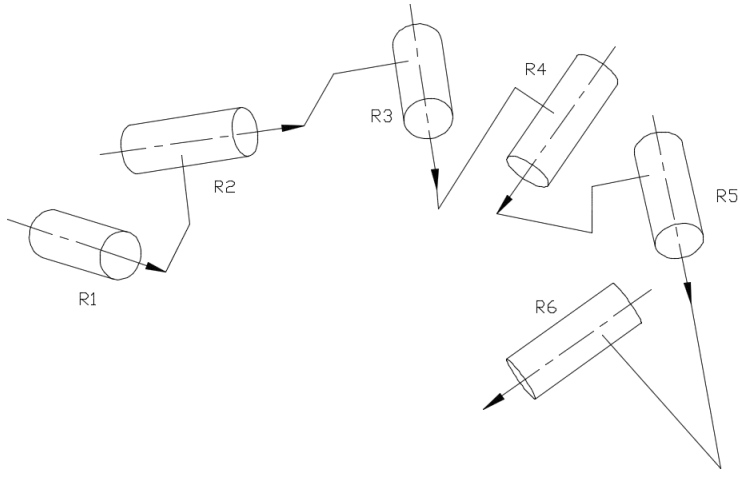

(a) General 6R serial mechanism

Fig. 6. 6R serial mechanism.

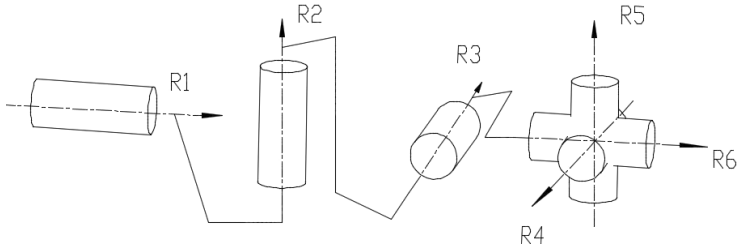

(b) 6R serial mechanism with orthogonal spherical joints

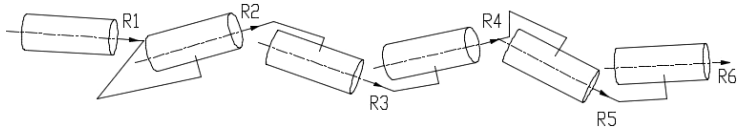

(c) Configuration of DOFs of the torso structure

Fig. 6. (*Continued*)

proposed torso structure for humanoid robot only retains the rotary joint and omits the link, which means that kinematic length (a) is equal to 0. When $a = 0$ and $\alpha \neq 0, \pi/2$ or π, it has special property of having no kinematic length for a link. The benefit of this design is that the structural volume is greatly reduced, and the compact and rigidity properties of torso structure are better.

The relative motion is called spherical when the intersecting joints are revolute. It can be easily seen from the sketch in Fig. 7, all points on link 3 move so that, relative to link 1, and they lie on concentric spheres centered at 0, the intersection point of the axes. Also, considering the single case, the relative positions of link 3 are limited to those which can be reached by pure rotation about axes through point 0. For the proposed torso structure, trajectories of a point in unit R6 are circles with different diameters by pure rotation about corresponding axes shown in Fig. 8, and they are located on two intersecting planes due to the location distributions of rotation axes.

However, coupling of six rotation axes determines actual movements of torso together. According to characteristics of the proposed torso structure, workspace analysis based on Monte Carlo method[27] of this mechanism can show geometric

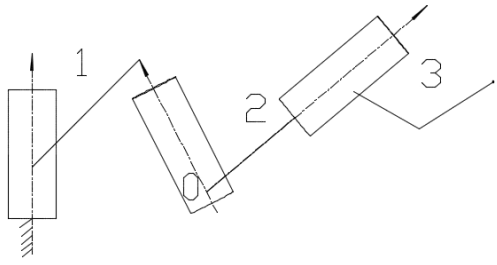

Fig. 7. A sketch of relative rotations.

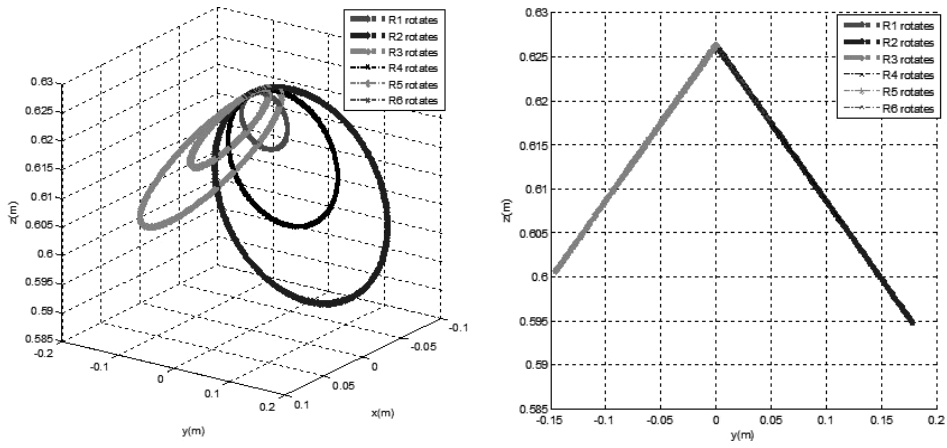

(a) x–y–z space (b) y–z plane

Fig. 8. Terminal trajectories under the circumstances of independent rotation of joints.

characteristics of the workspace boundary surface. Monte Carlo method has no limits to joint types (revolute or prismatic joints) and ranges of joint variables θ_i. It is assumed that $\theta_i = \theta_i^{\min} + (\theta_i^{\max} - \theta_i^{\min}) \times \text{Rand}()$. Values of all joints can yield individually in their rotation ranges by using a uniform pseudo-random number Rand(). Once the variation ranges are known, the workspace can be calculated. Algorithm is summarized as follows:

(1) Compute the location of point $P = [p_x, p_y, p_z]^T$ in forward kinematic.
(2) $\boldsymbol{W} = \emptyset$. The workspace is initialized as an empty set.
(3) **for** $\lambda = 1$ to 100,000 **do**.
(4) Randomly sample $\theta_i = \theta_i^{\min} + (\theta_i^{\max} - \theta_i^{\min}) \times \text{Rand}()$ in $[-\pi, \pi]$.
(5) Compute the position of point $\mathbf{P}$ in global coordinate system.

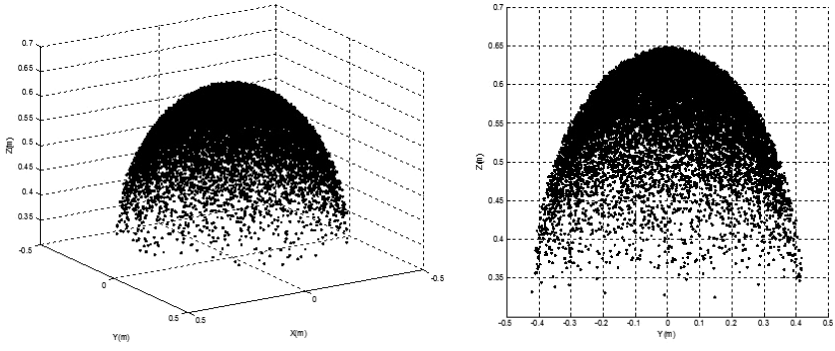

(a) x–y–z space (b) y–z plane

Fig. 9. Workspace of the proposed torso structure.

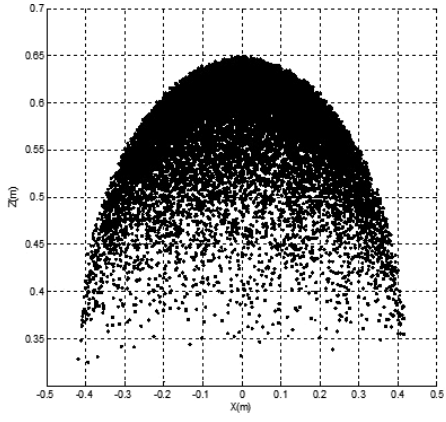

(c) x–z plane

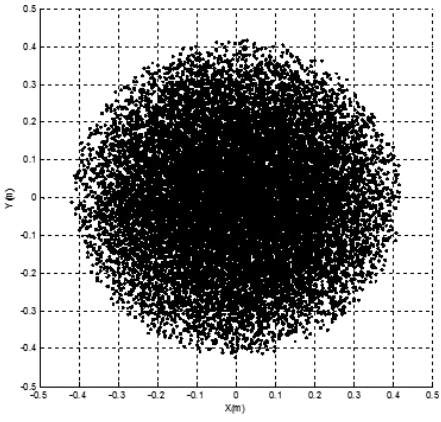

(d) x–y plane

Fig. 9. (*Continued*)

(6) Plot the point P in three-dimensional coordinate system, add **P** to $\boldsymbol{W}$.
(7) **end for**.

As can be seen from four perspectives in Fig. 9, geometric characteristic of the proposed torso structure's workspace is part of a sphere, it demonstrated that the proposed torso structure has the ability to achieve various motion patterns including rotation, bending and flexion, extension in 3D space.

The proposed torso structure is inspired by human spine, the purpose is to have good bionic performance with feasible operability. The quantitative bionic characteristics are decided by design parameters. Therefore, these design parameters of mechanism should be optimized for finding a practical feasible solution.

4. Bionic Optimization of Mechanism Design

The objective function method is widely used in kinematic optimization design of mechanism. This method is to solve optimization problems containing both equality and inequality constraints, it contains design variables, constraints and objective function.[28]

4.1. *Design variables*

The proposed torso structure is constituted by two kinds of basic units. Therefore, design parameters of these units decide the kinematic performance of torso structure. Design parameters of Modules 1 and 2 are shown in Fig. 10. d is the diameter of the output flange sleeve; φ is the angle between the output flange sleeve and the input flange cover; l is the height of unit from the harmonic reducer to the bottom of output flange sleeve. These parameters are important in motion characteristics of

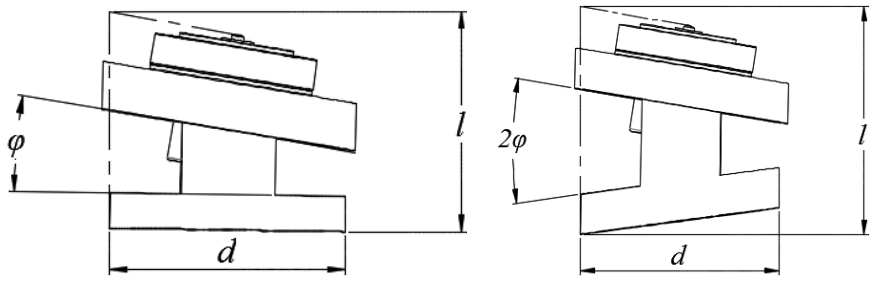

(a) Parameters of Module 1 (b) Parameters of Module 2

Fig. 10. Schematic diagram of structural parameters.

torso structure and selected as design parameters. For the convenience of expression, $\boldsymbol{x} = (x_1, x_2, x_3)^T = (\varphi, d, l)^T$.

4.2. *Objective function*

Right-bending is a typical motion pattern of human body. Human trunk moves in frontal plane during the right-bending procedure. But trajectory planning in joint space during the motion of right-bending procedure shows external displacements in positive x-axis direction of sagittal plane for the proposed torso structure (the z-axis is decided by right-hand rule). In Fig. 11, same linear drive function is applied to

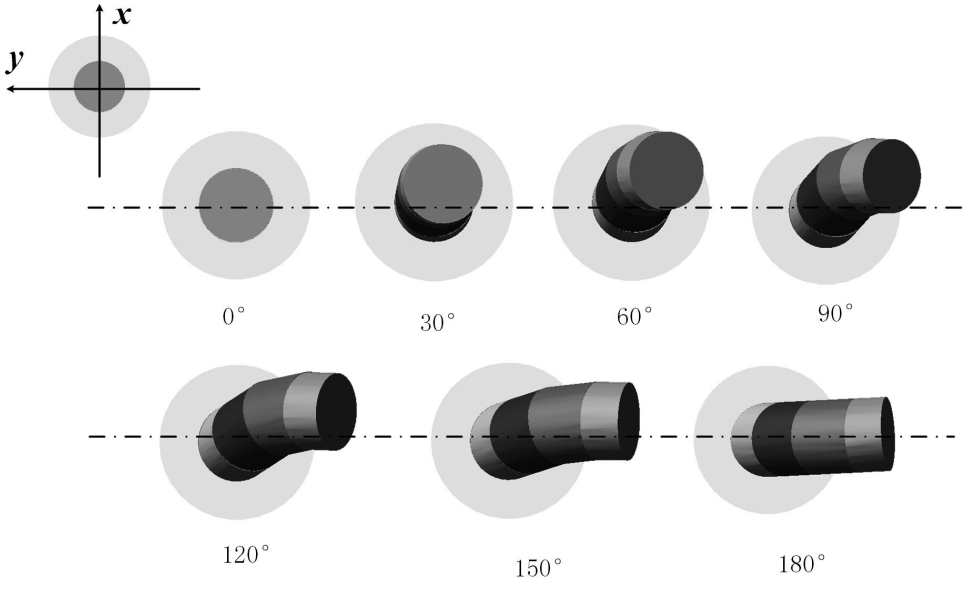

Fig. 11. Simulation snapshots of the 3D model operating the right-bending procedure in ADAMS environment. Rotation angles of each unit are marked below.

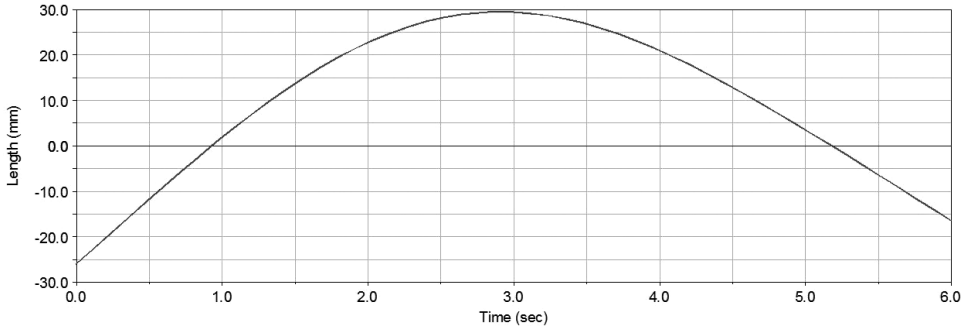

Fig. 12. Displacement of a point in R6 in x-axis.

each joint in ADAMS environment. It is demonstrated that the displacement component in the direction of x-axis is increasing from 0 to maximum at first, and then decreasing to 0 from the transverse plane of view in Fig. 12. It is necessary to reduce displacement in positive x-axis direction of sagittal plane, so the humanoid robots can move more naturally. Thus, it became the objective function to optimize the structure.

To calculate the mathematical expression of the displacement, forward kinematic of the proposed torso structure is presented. Figure 13(a) shows 3D outline drawing of torso structure with global coordinate system $x_0y_0z_0$ and D–H coordinate $x_1y_1z_1 - x_6y_6z_6$ systems. Only y- and z-axes are drawn, x-axis can be determined by right-hand rule. In Fig. 13(b), o_0, o_1, o', o'' are the midpoint of lines and z_0, z_1, z_2, z_3 axes are perpendicular to lines, respectively. It is not difficult to demonstrate that

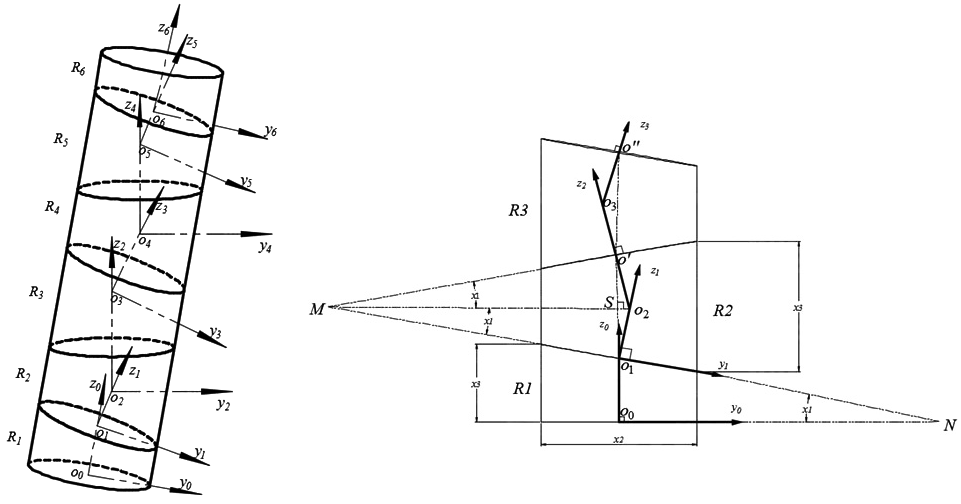

(a) Three-dimensional view (b) Frontal plane view

Fig. 13. Schematic diagram of configurations of DOFs and D–H coordinate systems.

Table 1. Parameters of torso structure of a humanoid robot.

#	θ	d	a	α
0-R1	θ_1	l_1	0	$-\varphi$
R1-R2	θ_2	l_2	0	2φ
R2-R3	θ_3	$2l_2$	0	-2φ
R3-R4	θ_4	$2l_2$	0	2φ
R4-R5	θ_5	$2l_2$	0	-2φ
R5-R6	θ_6	l_2	0	φ

$\mathrm{RT}\Delta MO'O_2 \cong \mathrm{RT}\Delta MO_1O_2$. So, it can be obtained that:

$$|O'O_1| = 2|O'S| = \frac{1}{2}[x_3 + (x_3 - 2x_2\tan x_1)] = x_3 - x_2\tan x_1. \tag{1}$$

In $\mathrm{RT}\Delta SO'O_2$, $\angle SO'O_2$ is equal to x_1:

$$|O'O_2| = \frac{|O'S|}{\cos\angle SO'O_2} = \frac{x_3 - x_2\tan x_1}{2\cos x_1}. \tag{2}$$

In $\mathrm{RT}\Delta NO_0O_1$:

$$|O_0O_1| = \frac{1}{2}[x_3 + (x_3 - x_2\tan x_1)] = x_3 - \frac{1}{2}x_2\tan x_1. \tag{3}$$

Some variables can be defined from the geometric relationship mentioned above to simplify the expressions:

$$l_1 = |O_0O_1| = x_3 - \frac{1}{2}x_2\tan x_1, \tag{4}$$

$$l_2 = |O_1O_2| = \frac{1}{2}|O_2O_3| = \frac{1}{2}|O_3O_4| = \frac{1}{2}|O_4O_5| = |O_5O_6| = \frac{x_3 - x_2\tan x_1}{2\cos x_1}. \tag{5}$$

Homogeneous transformation matrix[29] of positions between joint R_i and joint R_{i-1} $(i = 1 - 6)$ can be obtained with parameters listed in Table 1:

$$A_i = \begin{bmatrix} \cos\theta_i & -\sin\theta_i\sin\alpha_i & \sin\theta_i\sin\alpha_i & a_{i-1}\cos\theta_i \\ \sin\theta_i & \cos\theta_i\cos\alpha_i & -\cos\theta_i\sin\alpha_i & a_{i-1}\sin\theta_i \\ 0 & \sin\alpha_i & \cos\alpha_i & d_i \\ 0 & 0 & 0 & 1 \end{bmatrix}. \tag{6}$$

Position and orientation relations between $x_6y_6z_6$ and $x_0y_0z_0$ are the following:

$${}^0T_6 = A_1A_2A_3A_4A_5A_6 = \begin{bmatrix} n_x & o_x & a_x & p_x \\ n_y & o_y & a_y & p_y \\ n_z & o_z & a_z & p_z \\ 0 & 0 & 0 & 1 \end{bmatrix} = \begin{bmatrix} \boldsymbol{n} & \boldsymbol{o} & \boldsymbol{a} & \boldsymbol{p} \\ 0 & 0 & 0 & 1 \end{bmatrix}, \tag{7}$$

where $\boldsymbol{n}, \boldsymbol{o}, \boldsymbol{a}$ represent the orientation and $\boldsymbol{p}$ represents the position.

Position of point P in the global coordination system $x_0y_0z_0$:

$$\begin{bmatrix} P_i \\ 1 \end{bmatrix}_{x_0y_0z_0} = {}^0T_6 \begin{bmatrix} p_i \\ 1 \end{bmatrix}_{x_6y_6z_6}. \tag{8}$$

P_i and p_i represent positions of point P in global coordinate system and local coordinate system, respectively.

As shown in Fig. 12, displacement in sagittal plane during right-bending motion procedure reaches the maximum value at the time of third second. At this time, the joint variables are $[0, 0, -\frac{\pi}{2}, \frac{\pi}{2}, \frac{\pi}{2}, -\frac{\pi}{2}]$ for $\theta_1 - \theta_6$. And the value of $f(\boldsymbol{x}) = P_x(\theta_1, \theta_2, \theta_3, \theta_4, \theta_5, \theta_6, x_1, x_2, x_3)$ can be calculated as the objective function to optimize three design variables:

$$\begin{aligned} f(\boldsymbol{x}) = {} & (7\cos(x_1)\cos^2(2x_1)\sin(2x_1) - \cos(2x_1)\sin(2x_1))/200 + \sin(x_1) \\ & \times (x_3 - x_2\tan(x_1)) - 7\sin^2(2x_1)\sin(x_1)/200 - \cos(2x_1)\sin(x_1) \\ & \times (x_3 - x_2\tan(x_1)) + \sin(2x_1)\cos(x_1)(x_3 - x_2\tan(x_1)) \\ & + \cos(x_1)(\cos^2(2x_1)\sin(2x_1) - \cos(2x_1)\sin(2x_1))(x_3 - x_2\tan(x_1)/2) \\ & - \sin^2(2x_1)\sin(x_1) \times (x_3 - x_2\tan(x_1)/2) \\ & + \cos(2x_1)\sin(2x_1)\cos(x_1)(x_3 - x_2\tan(x_1)). \end{aligned} \tag{9}$$

This is a nonlinear equation with three variables.

4.3. *Constraints*

From the perspective of bionics, three constraints are set for structural design:

Firstly, the height of humanoid robot can be neither too high nor too short due to that humanoid robots are built to resemble human body and help people undertake various tasks in human society. Considering most presented humanoid robots' height, 1500 mm is chosen for the height of humanoid robot with the proposed torso. According to physiological data, the length of the torso accounts for 2/5 of the body height, which is 600 mm. To increase the value space of optimization, the total length of the proposed torso is between 600 mm and 635 mm. From Fig. 13(b) and Eqs. (1)–(3), it can be obtained that the total length of the proposed torso structure in vertical position is equal to:

$$2|O_0O_1| + 4|O'O_1| = 2\left(x_3 - \frac{1}{2}x_2\tan x_1\right) + 4(x_3 - x_2\tan x_1) = 6x_3 - 5x_2\tan x_1. \tag{10}$$

Extra 35 mm is set for the connection between head and trunk.

Secondly, the amplitude of bending motion for human is between 30° and 45°. A point P in unit R6 is chosen to be the measurement point shown in Fig. 14.

Thirdly, the basic geometrical dimensions of vertebral parts obtained from real values with digitized CT images have proportional relationship between the height and width as reported in Refs. 30 and 31. So the basic unit of the proposed torso

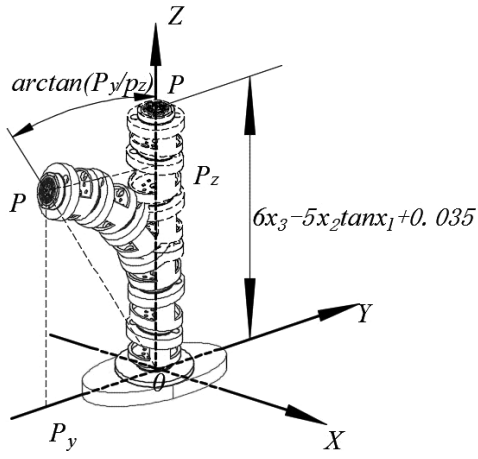

Fig. 14. Schematic diagram of constraints during right-bending.

structure adopted the proportional relationship varying from 1 to 1.2 for the length and the diameter.

It is concluded from the constraints mentioned above in mathematical expression:

$$\text{s.t.}\begin{cases} \dfrac{\pi}{6} \le \arctan\left|\dfrac{P_y}{P_z}\right| \le \dfrac{\pi}{4}, \\ 0.6 \le 6x_3 - 5x_2 \tan x_1 + 0.035 \le 0.635, \\ 1.0 \le \dfrac{x_2}{x_3} \le 1.2, \\ -x_i < 0 \quad (i = 1, 2, 3). \end{cases} \tag{11}$$

4.4. *Optimization results*

There are many optimization algorithms to objective function with inequality constraints such as trust region reflective algorithm, active set algorithm and interior point algorithm.[32] Trust region reflective algorithm is for optimization with linear equality constrains, which is not the suitable one. Interior point algorithm has higher computational efficiency with fewer iteration steps compared to active set algorithm. Algorithm is not discussed in detail in this paper, *fmincon* solver which is very mature and stable in Matlab environment is used to solve the problem with interior point algorithm, and the optimization results shown in Table 2 are obtained in 0.067 s.

Table 2. Optimized parameters.

Design parameters	φ	d	l
Optimized parameters	8.3°	132.3 mm	110.3 mm

Population parameters of the proposed torso structure can be obtained from these basic parameters: the total length is 600.1 mm, the amplitude of right-bending is 30.0°, and the minimum value of the objective function is 47.8 mm. The goal of bionic optimization design has been achieved within constraints.

5. Simulation of Right-Bending Motion

The motion feasibility has been simulated both to get joint ranges for design purposes and to check the motion of torso. For a practical application of a simulation, the trajectory between two prescribed points can be computed in joint space by using a quintic polynomial function[33,34]:

$$\theta(t) = c_0 + c_1 t + c_2 t^2 + c_3 t^3 + c_4 t^4 + c_5 t^5, \tag{12}$$

where $\theta(t)$ is the prescribed trajectory of joint variable as a function of time.

The six unknown constant values can be determined by solving six constraints equations, which are given by the values of six boundary conditions including angles, velocities and accelerations at the starting and end positions:

$$\begin{aligned} \boldsymbol{\theta}(t_0) &= \boldsymbol{\theta}_0 \quad \boldsymbol{\theta}(t_f) = \boldsymbol{\theta}_f, \\ \dot{\boldsymbol{\theta}}(t_0) &= \dot{\boldsymbol{\theta}}_0 \quad \dot{\boldsymbol{\theta}}(t_f) = \dot{\boldsymbol{\theta}}_f, \\ \ddot{\boldsymbol{\theta}}(t_0) &= \ddot{\boldsymbol{\theta}}_0 \quad \ddot{\boldsymbol{\theta}}(t_f) = \ddot{\boldsymbol{\theta}}_f, \end{aligned} \tag{13}$$

$$\begin{aligned} c_0 &= \theta_0, \quad c_1 = \dot{\theta}_0, \quad c_2 = \frac{1}{2}\ddot{\theta}_0, \\ c_3 &= \frac{1}{2t_f^3}[20(\theta_f - \theta_0) - (8\dot{\theta}_f + 12\dot{\theta}_0)t_f - (3\ddot{\theta}_0 - \ddot{\theta}_f)t_f^2], \\ c_4 &= \frac{1}{2t_f^4}[30(\theta_0 - \theta_f) + (14\dot{\theta}_f + 16\dot{\theta}_0)t_f + (3\,\ddot{\theta}_0 - 2\,\ddot{\theta}_f)t_f^2], \\ c_5 &= \frac{1}{2t_f^5}[12(\theta_f - \theta_0) - 6(\dot{\theta}_f + \dot{\theta}_0)t_f - (\ddot{\theta}_0 - \ddot{\theta}_f)t_f^2], \end{aligned} \tag{14}$$

where t_0 and t_f are the initial and end time of simulation.

The boundary conditions of the quintic polynomial trajectories are shown below, time is assumed to vary from 0 s to 10 s in 1000 steps:

$$\begin{aligned} &\boldsymbol{\theta}_0 = \dot{\boldsymbol{\theta}}_0 = \ddot{\boldsymbol{\theta}}_0 = [0, 0, 0, 0, 0, 0], \\ &\boldsymbol{\theta}_f = [0, 0, -\pi, \pi, \pi, -\pi], \\ &\dot{\boldsymbol{\theta}}_f = \ddot{\boldsymbol{\theta}}_f = [0, 0, 0, 0, 0, 0], \\ &t_0 = 0\,\text{s}, \\ &t_f = 10\,\text{s}. \end{aligned} \tag{15}$$

Simulations have been carried out to evaluate and to characterize the right-bending performances of the proposed torso structure in Fig. 15. The simulations

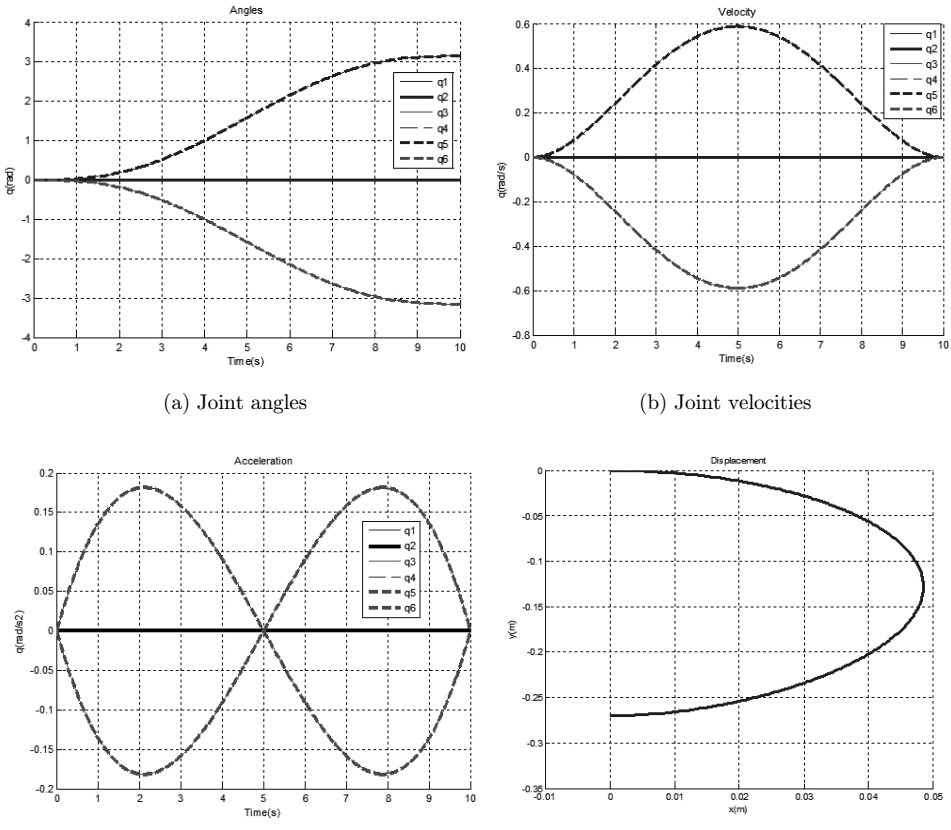

(a) Joint angles

(b) Joint velocities

(c) Joint accelerations

(d) Displacement in X–Y plane

Fig. 15. Computed joint variables for right-bending motion.

show a smooth motion which well imitate the movements of human torso during the right-bending motion procedure.

The orientation of robots are usually defined by a rotation sequence around x-, y- and z-axes. ϕ, θ, ψ are used to present three basic rotations around x-axis, y-axis and z-axis respectively, namely are roll, pitch and yaw. The order of rotations is defined as

$$\begin{aligned} RPY(\phi,\theta,\psi) &= \mathrm{Rot}(z,\phi)\mathrm{Rot}(y,\theta)\mathrm{Rot}(x,\psi) \\ &= \begin{bmatrix} c\phi c\theta & c\phi s\theta s\psi - s\phi c\psi & c\phi s\theta c\psi + s\phi s\psi & 0 \\ s\phi c\theta & s\phi s\theta s\psi + c\phi c\psi & s\phi s\theta c\psi - c\phi s\psi & 0 \\ -s\theta & c\theta s\psi & c\theta c\psi & 0 \\ 0 & 0 & 0 & 1 \end{bmatrix}, \end{aligned} \tag{16}$$

where $s\theta$ is for $\sin\theta$, and $c\theta$ is for $\cos\theta$ and so on. Generally, it is called Roll-Pitch-Yaw method.

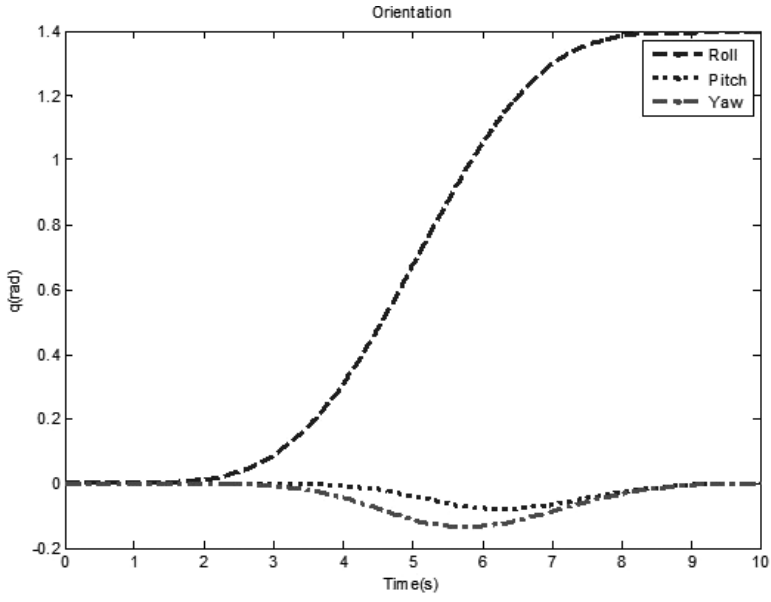

Fig. 16. Computed orientation angles for a simulated operation of right-bending motion.

The changes of orientation angles of the proposed torso structure are shown in Fig. 16. The torso rotates 80.21° around its roll axis and nearly 0° around its pitch and yaw axes. Since the stable orientation of the proposed torso, the head of humanoid robot can well imitate the right-bending motion with human-like motion characteristics. It is noted that the proposed torso structure is very well designed as the torso structure for humanoid robots.

For the proposed torso structure, right-bending motion is representative in three typical movement patterns due to the brilliant property of symmetry. Take the flexion movement in sagittal plane as an example, rotate unit R1 counter-clockwise for 90° and rotate the head in R6 clockwise for 90° from the top of view at first, the robot stays still during the process. After that, the trajectory planning of right-bending motion in joint space mentioned above can be applied to achieve flexion movement in sagittal plane.

6. Conclusion

A new torso structure for humanoid robots has been proposed based on general six revolute serial mechanism. The proposed system with six DOFs shows high stiffness, high DOFs, self-locking capabilities as well as easy-to-control features with anthropomorphic characteristics. Bionic optimization design based on objective function method has been implemented for better motion performances. A 3D model has been elaborated and simulated in SolidWorks and ADAMS environments respectively to check practical motion feasibility. Simulations of right-bending motion in Matlab

environment show that the proposed torso structure can well imitate motions of human torso with feasible operation performances for humanoid robots.

Acknowledgments

This work was supported by the National Natural Science Foundation of China (Nos. 51405469 and 61401437).

References

1. M. Hirose, Y. Haikawa, T. Takenaka and K. Hirai, Development of humanoid robot ASIMO, in *IEEE/RSJ Int. Conf. Intelligent Robots and Systems* (*IROS*) (IEEE Press, Maui, USA, 2001), pp. 1–6.
2. J. H. Kim and J. H. Oh, Realization of dynamic walking for the humanoid robot platform KHR-1, *Adv. Robot.* **18**(7) (2004) 749–768.
3. I. W. Park, J. Y. Kim, S. W. Park *et al.*, Development of the humanoid platform KHR-2, *Int. J. Hum. Robot.* **2**(4) (2005) 519–536.
4. I. W. Park, J. Y. Kim, J. Lee and J. H. Oh, Mechanical design of humanoid robot platform KHR-3 (KAIST Humanoid Robot 3: HUBO), in *IEEE–RAS Int. Conf. Humanoid Robots* (IEEE Press, Tsukuba, Japan, 2005), pp. 321–326.
5. I. W. Park, J. Y. Kim, J. Lee and J.-H. Oh, Mechanical design of the humanoid robot platform, HUBO, *Adv. Robot.* **21**(11) (2007) 1305–1322.
6. K. Yokoi, N. Kawauchi, N. Sawasaki *et al.*, Humanoid robot applications in HRP, *Int. J. Hum. Robot.* **1**(3) (2004) 409–428.
7. K. Kaneko, K. Harada *et al.*, Humanoid robot HRP-3, in *IEEE/RSJ Int. Conf. Intelligent Robots and Systems* (IEEE Press, Nice, 2008), pp. 2471–2478.
8. K. Kaneko, F. Kanehiro *et al.*, Cybernetic human HRP-4C, in *IEEE–RAS Int. Conf. Humanoid Robots* (IEEE Press, Paris, France, 2009), pp. 7–14.
9. A. Parmiggiani, M. Maggiali, L. Natale *et al.*, Design of the iCub humanoid robot, *Int. J. Hum. Robot.* **9**(4) (2012) 1250027.
10. Y. Ogura, H. Aikawa *et al.*, Development of a new humanoid robot WABIAN-2, in *IEEE Int. Conf. Robotics and Automation* (*ICRA*) (IEEE Press, Orlando, USA, 2006), pp. 76–81.
11. T. Siedel, M. Hild and M. Weidner, Concept and design of the modular actuator system for the humanoid robot MYON, in *Int. Conf. Intelligent Robotics and Applications* (*ICIRA*) (Springer, Berlin, 2011), pp. 388–396.
12. X. Zhao, Q. Huang, Z. Peng *et al.*, Kinematic mapping of humanoid motion based on human motion, *Robotics* **27**(4) (2005) 358–361.
13. S. Chen, H. Shen and B. Chen, Kinematic analysis and simulation of squatting down and lifting object for humanoid robot, in *IEEE Int. Conf. Robotics and Biomimetics* (*ROBIO*) (IEEE Press, Shenzhen, China, 2013), pp. 2732–2736.
14. J. Or and A. Takanishi, A biologically-inspired CPG-ZMP control system for the real-time balance of a single-legged belly dancing robot, in *IEEE/RSJ Int. Conf. Intelligent Robots and Systems* (IEEE Press, Sendai, Japan, 2004), pp. 931–936.
15. J. Greenman, O. Holland, I. Kelly *et al.*, Towards robot autonomy in the natural world: A robot in predator's clothing, *Mechatronics* **13**(3) (2003) 195–228.
16. V. Potkonjak, B. Svetozarevic, K. Jovanovic and O. Holland, The puller-follower control of compliant and noncompliant antagonistic tendon drives in robotic system, *Int. J. Adv. Robot. Syst.* **8**(5) (2012) 143–155.

17. I. Mizuuchi, T. Yoshikai, Y. Sodeyama *et al.*, A musculoskeletal flexible-spine humanoid Kotaro aiming at the future in 15 years time, in *Mobile Robots Towards New Applications* (INTECH Open Acess Publisher, 2006).
18. I. Mizuuchi, Y. Nakanishi, Y. Sodeyama *et al.*, An advanced musculoskeletal humanoid Kojiro, in *IEEE–RAS Int. Conf. Humanoid Robots* (IEEE Press, Pittsburgh, USA, 2007), pp. 294–299.
19. Y. Asano, H. Mizoguchi, T. Kozuki *et al.*, Lower thigh design of detailed musculoskeletal humanoid "Kenshiro", in *IEEE/RSJ Int. Conf. Intelligent Robots and Systems* (IEEE Press, Vilamoura, Portugal, 2012), pp. 4367–4372.
20. D. Cafolla and M. Ceccarelli, Design and simulation of a cable-driven vertebra-based humanoid torso, *Int. J. Hum. Robot.* **13**(4) (2016) 1650015.
21. I. Georgials and V. Tourassis, From the human spine to hyper-redundant robots: The ERMIS mechanism, *ISRN Robot.* **2013** (2013) 890609, 9 pp.
22. P. Yao, T. Li, M. Luo and Q. Zhang, Analysis of human spine functionality from the perspective of humanoid robots, in *IEEE Int. Conf. Mechatronics and Automation* (IEEE Press, Harbin, China, 2016), pp. 1167–1172.
23. T. Aydin, *Human Body Dynamics: Classical Mechanics and Human Movement* (Springer-Verlag, New York, 2000), pp. 1–10.
24. J. A. William, F. D. William *et al.*, Cervical motion segment contributes to head motion during flexion/extension, lateral bending, and rotation, *Spinal J.* **15**(12) (2015) 2538–2543.
25. L. S. Lippert, *Clinical Kinesiology and Anatomy*, 4th edn. (F. A. Davis Company, Philadelphia, 2006), pp. 184–228.
26. Z. Wang, D. Zhang, Y. An *et al.*, Inverse kinematics analysis of the 6R serial spraying manipulator with non-spherical wrist, *J. Tianjin Univ.* **40**(6) (2007) 665–670.
27. A. Peidró, A. Gil, J. M. Marín *et al.*, *Monte Carlo Workspace Calculation of a Serial-Parallel Biped Robot in Robot 2015: Second Iberian Robotics Conf.* (Springer International Publishing, 2016).
28. E. K. P. Chong and S. H. Żak, *An Introduction to Optimization*, 4th edn. (Wiley, UK, 2013), pp. 525–610.
29. Z. Cai, *Robotics*, 2nd edn. (Tsinghua University Press, Beijing, 2011), pp. 42–60.
30. M. Ceccarelli, R. C. Saltarelo, G. Carbone and J. C. M. Carvalho, Simulation of the lumbar spine as a multi-module parallel manipulator, *Appl. Bionics Biomech.* **8**(3–4) (2011) 399–410.
31. S. H. Zhou, I. D. McCarthy, A. H. McGregor *et al.*, Geometrical dimensions of the lower lumbar vertebrae — Analysis of data from digitized CT images, *Eur. Spine J.* **9**(3) (2000) 242–248.
32. C. Gong and Z. Wang, *Proficient MATLAB Optimization Calculation* (Electronic Industry Press, Beijing, 2015), pp. 78–92.
33. H. Dong, *Principle and Technology of Robots* (Tsinghua University Press, Beijing, 2014), pp. 125–162.
34. C. Liang and M. Ceccarelli, Design and simulation of a waist-trunk system for a humanoid robot, *Mech. Mach. Theory* **53** (2010) 50–65.

Peng Yao received the B.Sc. degree in 2014 from Shenyang Aerospace University and he is working towards the M.Sc. degree in Mechanical Engineering in the Department of Precision Machinery and Precision Instrumentation, University of Science and Technology of China. His major research is in humanoid robots.

Tao Li is currently an Associate Researcher at Hefei Institutes of Physical Science, Institute of Advanced Manufacturing Technology, Chinese Academy of Sciences. He received his Ph.D. degree in Mechanical Engineering from the University of Cassino, Italy in 2012. His major research covers humanoid robots and personal robots.

Minzhou Luo is currently a Researcher at Hefei Institutes of Physical Science, Chinese Academy of Sciences. He received his Ph.D. degree in Pattern Recognition and Intelligent Systems from the University of Science and Technology of China in 2005. His major research covers biomimetic robots, humanoid robots, industrial robots, intelligent machinery, and mechatronics.

Qingqing Zhang received the B.Sc. degree in 2014 from Anhui University of Science and Technology, and she is working towards the M.Sc. degree in Mechanical Engineering in the Department of Precision Machinery and Precision Instrumentation, University of Science and Technology of China. Her major research is in humanoid robots.

Zhiying Tan is currently a Research Assistant at Hefei Institutes of Physical Science, Institute of Advanced Manufacturing Technology, Chinese Academy of Sciences. She received her Ph. D. degree in Computer Software and Theory from the University of Electronic Science and Technology of China in 2013. Her major research covers numerical analysis, image processing and machine vision.